Journal of Soft Computing in Civil Engineering 8-4 (2024) 160-185

Contents lists available at SCCE

Journal of Soft Computing in Civil Engineering

Journal homepage: www.jsoftcivil.com

Axial Capacity Estimation of FRP-Strengthened Corroded Concrete Columns

Chandan Gupta [1]; Harish Chandra Arora [2,3]; Aman Kumar [2,3,*]; Prashant Kumar [2,3,4]; Nishant Raj Kapoor [2]; Madhu Sharma [1]

1. Department of Civil Engineering, Jawaharlal Nehru Government Engineering College, Sunderngar, 175018, India
2. AcSIR—Academy of Scientific and Innovative Research, Ghaziabad 201002, India
3. Structural Engineering Department, CSIR—Central Building Research Institute, Roorkee, 247667, India
4. Department of Civil Engineering, COER University, Roorkee, 247667, India

* Corresponding author: *aman.civil16@outlook.com*

https://doi.org/10.22115/scce.2024.414586.1708

ARTICLE INFO

Article history:
Received: 02 September 2023
Revised: 17 December 2023
Accepted: 23 February 2024

Keywords:
RC column;
Corrosion;
Axial capacity;
Machine learning;
FRP;
ANN;
GPR;
SVM.

ABSTRACT

This research presents a machine learning (ML) based model to estimate the axial strength of corroded RC columns reinforced with fiber-reinforced polymer (FRP) composites. Estimating the axial strength of corroded columns is complex due to the intricate interplay between corrosion and FRP reinforcement. To address this, a dataset of 102 samples from various literature sources was compiled. Subsequently, this dataset was employed to create and train the ML models. The parameters influencing axial strength included the geometry of the column, properties of the FRP material, degree of corrosion, and properties of the concrete. Considering the scarcity of reliable design guidelines for estimating the axial strength of RC columns considering corrosion effects, artificial neural network (ANN), Gaussian process regression (GPR), and support vector machine (SVM) techniques were employed. These techniques were used to predict the axial strength of corroded RC columns reinforced with FRP. When comparing the results of the proposed ML models with existing design guidelines, the ANN model demonstrated higher predictive accuracy. The ANN model achieved an R-value of 98.08% and an RMSE value of 132.69 kN which is the lowest among all other models. This model fills the existing gap in knowledge and provides a precise means of assessment. This model can be used in the scientific community by researchers and practitioners to predict the axial strength of FRP-strengthened corroded columns. In addition, the GPR and SVM models obtained an accuracy of 98.26% and 97.99%, respectively.

How to cite this article: Gupta C, Arora HC, Kumar A, Kumar P, Kapoor NR, Sharma M. Axial capacity estimation of FRP-strengthened corroded concrete columns. J Soft Comput Civ Eng 2024;8(4):160–185. https://doi.org/10.22115/scce.2024.414586.1708

2588-2872/ © 2024 The Authors. Published by Pouyan Press.

This is an open access article under the CC BY license (http://creativecommons.org/licenses/by/4.0/).

1. Introduction

Columns play a vital role in a building's structure as they bear the weight of the upper parts and transmit it to the ground. They are responsible for maintaining the stability of the structure over a long period, even when facing challenges like earthquakes or strong forces. However, the ability of these load-bearing columns to support weight can decrease significantly over time if they are exposed to corrosive environments. This can lead to a reduction in their overall strength and lifespan [1,2]. When gases like CO_2, sulphur, and chloride penetrate the concrete through the voids, they trigger corrosion in the steel reinforcement. A coating of ferric oxide forms on the surface of reinforcement when corrosion begins. Rust generates internal pressure that damages the surrounding concrete since it takes up more space than steel does. The production of several layers of ferric oxide on the reinforcement exerts significant strain on the nearby concrete and causes hair-line to large fractures. There is a significant reduction in the connection between concrete and reinforcement [3]. The process of corrosion generally occurs due to the carbonation phenomenon and ingress of chlorides in concrete. In the carbonation mechanism, the carbon dioxide gas from the atmosphere attacks the steel rebar which initiates corrosion in steel rebar. The penetrated carbon dioxide destroys the alkalinity of concrete, eventually reduces the pH of concrete and diminishes the passivity of steel rebar. Chlorides from the coastal environment ingress into concrete due to which the de-passivation of the steel rebar occurs. The cover concrete begins to peel off as a result of a weakening of the link between the steel and concrete. At this point, the diameter of the bar gets reduced. The primary bars buckle as a result of the cover concrete spalling and ties cracking, which causes the concrete in that area to bulge [4,5].

The deterioration of structures played a vital role in affecting the service life of the buildings. Demolishing of buildings is not a feasible solution as it produces a large amount of debris. However, retrofitting of structural elements may be the optimal solution in the construction industry. Numerous research on the use of fiber-reinforced polymer (FRP) wrapping not only shield but also strengthen the corroded reinforced concrete (RC) columns during the past two decades [6,7]. The service life and durability of the RC columns can be improved by FRP wrapping, which also gives the column extra strength and protection. According to studies, FRP wrapping enhances the axial load-carrying ability of the deteriorated RC columns [8,9]. There are several types of FRP that can be used to strengthen the RC columns. The most common types of FRP materials are carbon FRP (CFRP), glass FRP (GFRP), basalt FRP (BFRP), and aramid FRP (AFRP). When it comes to wrapping techniques, there are two primary methods: wet layup and pre-cured. Another wrapping technique is called the hybrid method, which involves combining two or more types of FRP materials to create a customized reinforcement system. FRP presents numerous benefits to the construction industry, such as an enhanced weight-to-strength ratio, resistance to corrosion, easy installation, lightweight properties, and high durability. The lightweight nature of FRP contributes to cost-effective construction with increased efficiency. However, it is important to note that the performance of FRP diminishes when exposed to elevated temperatures, posing a significant challenge. At higher temperatures, the epoxy resin embedding high-strength fibers undergoes a liquid-glass transition, impacting the overall effectiveness of FRP.

There is a scarcity of global empirical models in the structural engineering domain for predicting the axial strength capacity of columns that have experienced corrosion and are reinforced with FRP wrapping. Moreover, analytical models and design guidelines are based on mathematical equations that describe the behaviour of the system being studied. These models are usually built using fundamental principles and rely on prior knowledge of the system being studied, including its properties and boundary conditions. Analytical models are limited to the assumptions and simplifications made in the model. These are generally inflexible and require significant effort to modify or update. Conversely, machine learning (ML) is a swiftly advancing domain that employs algorithms and statistical models to make decisions grounded in data. To uncover patterns and create forecasts using statistical reasoning, ML models are built by training algorithms on extensive datasets. By scrutinizing past information about structural breakdowns and their underlying reasons, ML algorithms can pinpoint patterns and anticipate potential occurrences of failures. These algorithms can handle intricate and non-linear connections between factors, and they can be effortlessly adjusted by retraining them with fresh data. The ML models can assist engineers and construction firms in taking proactive steps to stop problems before they happen, resulting in structures that are safer and more dependable. It improves the speed, precision, and security of building projects.

Previously published studies focussed on the estimation of compressive strength and axial capacity of columns confined with FRP using ML algorithms without taking corrosion factor in consideration which reflect the major limitations of the published work. The primary objective of this research is to evaluate the ability of ML algorithms to determine the axial load-carrying capability of corroded RC columns that have been reinforced with FRP. This study is the first attempt that consider the corrosion factor in predicting axial capacity of FRP-strengthened columns using ML techniques. The ML techniques used in this study include artificial neural network (ANN), Gaussian process regression (GPR), and support vector regression (SVR). The employed ML models fill the existing gap in knowledge that has not been considered yet. Furthermore, the investigation aimed to uncover the impact of various input parameters on the axial load-carrying capacity of these columns.

2. Literature review

In a study conducted by Naderpour et al. [10], a model was put forth to predict the compressive strength of circular RC columns reinforced with FRP. They employed a neuro-fuzzy model called the adaptive neuro-fuzzy inference system (ANFIS). The research drew from an experimental dataset consisting of 95 cases, and only two models were presented and compared. The findings of the study highlighted that the proposed ANFIS model outperformed other ML methods. Through sensitivity analysis, it was revealed that changes in the column's height and the yield strength of the longitudinal steel had the most significant influence on the model's output. The study also determined that the column's load-carrying capacity increased when the yield strength of the longitudinal steel surpassed a specific threshold value. Ghanem and Elgazzar [11] crafted a model to determine the axial compressive strength and axial strain of circular concrete columns that are reinforced with both FRP and internal steel. They explored two methods for analyzing the columns without causing damage, namely ANN and regression

analysis (RA). Based on their experiments, the developed ANN model displayed a strong ability to predict the compressive stress and strain of the columns with a high degree of accuracy and only minor discrepancies. The research revealed that the lateral pressure created by the reinforcing fibers played the most significant role in determining the compressive strength and strain of the columns, whereas the transverse steel's impact on the confined column's compressive strength was relatively small.

Raza et al. [12] introduced 18 distinct models using ANN to forecast the ability RC columns wrapped with FRP to carry axial loads. Among these models, the ANN model, with 11 neurons in the first hidden layer and 11 neurons in the second hidden layer, displayed results that were closely matched with experimental outcomes. The performance metrics showed a coefficient of determination (R^2) of 0.921, mean squared error (MSE) of 0.32, and mean absolute error (MAE) of 1.82. A study examining various parameters using the proposed empirical model revealed that the axial load-carrying capacity of GFRP-RC columns rises notably with increases in the concrete column's cross-sectional area and compressive strength. The impact of the tensile strength and reinforcement ratio of longitudinal GFRP bars on the axial capacity of GFRP-strengthened concrete columns was found to be negligible. Bakouregui et al. [13] introduced a novel approach to estimate the load-carrying capability of RC columns strengthened with FRP. They utilized an advanced algorithm known as eXtreme Gradient Boosting (XGBoost) along with the SHAP (Shapley additive explanation) framework. The developed XGBoost model was built upon a dataset of 283 experimental results from FRP-strengthened concrete columns. In this model, thirteen different factors were considered as input data, and the SHAP algorithm was applied to assess the significance and contributions of each factor. Among the input factors, those that held the most weight in determining the outcome were the eccentricity ratio, the overall cross-sectional area, the concrete's compressive strength, the slenderness ratio, and the spacing or arrangement of transverse reinforcement. When dealing with shorter columns, the XGBoost model displayed promising performance metrics on the testing set, with average values of 0.977 for R^2, 218.7 kN for root mean square error (RMSE), 137.5 kN for MAE, and 5.3% for mean absolute percentage error (MAPE). In a study by Radhi et al. [14], an examination was conducted on the load-carrying and strain capacities of columns, both those without confinement and those reinforced with CFRP. The researchers concluded that wrapping corroded columns with two layers of CFRP was more effective in boosting their strength capacity and ultimate axial strain in comparison to using one CFRP layer. They also unveiled that as the number of CFRP layers increased, the axial compressive strength capacity of the columns also increased. Conversely, this strength capacity decreased with higher levels of corrosion. The study provided a practical recommendation suggesting that reinforcing the regions of the column near its supports could effectively prevent extreme stress concentrations, enhancing the overall stability of the structure. Bae and Belarbi [15] found that although CFRP wrapping couldn't completely arrest the corrosion process, it significantly reduced the corrosion rate in columns when compared to those without any wrapping. This suggested that moisture could still enter the concrete through absorption and then spread via diffusion through the matrix resin and the parts of the columns that were not covered by the CFRP wrapping. The research conducted by Lee et al. [16] focused on enhancing the condition of columns damaged by corrosion using CFRP sheets. Their study demonstrated that this method significantly enhanced the strength and

flexibility of the corroded column. Remarkably, the load-carrying capacity of the corroded column increased by 28% after the application of CFRP sheets. The study also found that this treatment effectively curtailed the occurrence of corrosion after repair. Specifically, there was a substantial 50% reduction in the corrosion rate following the wrapping process, along with a similar decrease in the natural corrosion currents.

Mohammed et al. [17] developed a model that accurately anticipated the ultimate axial load capacity of RC columns that had experienced damage and were then repaired using an FRP jacket. This model proves quite beneficial for gauging the extent of damage that the FRP jacket can rectify in terms of the structural soundness of a weakened column. Their investigation revealed that the GFRP jacket was notably successful in restoring the axial load capacity of the RC columns. In cases of 25% and 50% corrosion damage, the GFRP jacket managed to restore the column's axial load capacity by 99% and 95%, respectively. This repair system effectively stabilized and restored the strength of the damaged columns. Furthermore, the study concluded that the GFRP jacket's efficacy was more pronounced in the repair of circular columns when compared to square columns.

The square column with damage displayed a 43% lower axial load capacity than that of the circular counterpart. This difference arose due to stress concentration at the corners of the square section, especially where joints were located. Zhou et al. [18] carried out a practical study on RC columns that were corroded and strengthened with FRP material. Their investigation demonstrated that using an external FRP jacket to reinforce corroded RC columns brought about noteworthy improvements in their mechanical abilities, regardless of the level of corrosion. Importantly, this retrofitting technique was notably more effective for enhancing the performance of existing corroded RC columns in comparison to newly constructed ones. The study findings also emphasized that the application of externally wrapped FRP jackets had a more pronounced impact on enhancing the structural capabilities of severely corroded columns. Tastani and Pantazopoulou [19] investigated that CFRP jackets consistently outperformed GFRP jackets due to CFRP's superior mechanical properties. However, it was observed that GFRP led to a more favorable, nearly ductile behavior after reaching the peak load.

Kashi et al. [20] conducted a hands-on study to rehabilitate corroded RC columns using various techniques involving the application of FRP sheets. Their findings revealed that when exposed to marine conditions, the immediate effectiveness of retrofitting columns with a single layer of CFRP was quite promising. Interestingly, columns reinforced using a single layer of GFRP exhibited superior performance compared to the other tested methods. The study led to the conclusion that in challenging environmental conditions, relying solely on using durable types of FRP sheets for wrapping wouldn't be enough. Instead, safeguarding the outer surface of the FRP sheets would need to be taken into account for effective long-term results. Debaiky et al. [21] developed a model capable of forecasting how columns would react under stress and strain when various combinations of external FRP wraps and internal transverse reinforcement were employed. The model demonstrated particular utility in predicting the behavior of columns in such scenarios. In instances where FRP wraps were applied to corroded columns, the study found that a reduction factor of 50% for the cover thickness aligned well with the experimental

outcomes. When assessing the load-carrying capability, it was established that a corroded and unrepaired column could manage 38% less load than an undamaged column. This was in line with both the numerical routine results, which highlighted the impact of reduced concrete cover strength, and the experimental findings, which showed a 30% decrease.

Pantazopoulou et al. [22] delved into the effectiveness and efficiency of using FRP wraps as a substitute for traditional repair methods in addressing corrosion-induced damage in RC columns. They carried out experiments on a set of small-scale concrete columns, each featuring different reinforcement arrangements. The research showcased that by increasing the number of FRP layers and ensuring proper anchorage by overlapping the ends, the columns' performance exhibited significant enhancement. Among the various repair alternatives tested, the most effective and straightforward approach involved cleaning the damaged surface without removing the contaminated or cracked cover concrete. This method entailed applying layers of fiber-reinforced composite wraps directly onto the columns. This option proved to be both highly effective and easy to execute.

In this study, the established guidelines for constructing and designing structural concrete that incorporates FRP reinforcement, such as ACI 440.2R--08 [23], ACI 318-05 [24], and IS 456: 2000 [25], are used as a basis. These guidelines are applied to evaluate the axial load-carrying capacity of RC columns that have been affected by corrosion and subsequently reinforced with FRP materials.

2.1. Research significance

Anticipating the axial load-carrying capacity of corroded and FRP-strengthened RC columns holds immense significance for safeguarding both the structure and its occupants. Such predictions offer the chance to optimize designs, minimize unnecessary material usage, and reduce costs tied to construction. Ensuring the accurate estimation of load capacity in repaired columns helps guarantee that the structure aligns with necessary performance benchmarks and standards. Current literature reveals a gap in comprehensive prediction models specifically designed to provide dependable estimates for the axial load capacity of RC columns, especially when they've undergone corrosion and subsequent FRP reinforcement. This manuscript strives to address this gap and pioneers an exploration into the axial load-bearing capacity of RC columns affected by corrosion and reinforced using FRP composites. The unique methodology employed here involves the application of ML algorithms, with a focused emphasis on scenarios where the load is evenly centered. The resultant model crafted in this study is distinct for its simplicity, high accuracy, dependability, user-friendliness, and thoroughness in evaluating the axial load-bearing capability of RC columns that have endured corrosion and are strengthened with FRP.

3. Artificial intelligence

Artificial intelligence (AI) involves creating computer systems that can learn, solve problems, perform tasks, and process language in a way similar to human thinking. ML is the domain of AI that employs algorithms to analyze data, making predictions by identifying patterns and connections within the data. This is a significant advancement in the AI field. Neural networks,

which mimic the human brain, are integral to both ML and deep learning algorithms. Deep learning, a type of ML, imitates the functions of the human brain. AI finds application in various areas, such as self-driving cars and personal digital assistants like Siri and Alexa.

3.1. Machine learning

ML is a branch of AI and computer science that harnesses data and algorithms to replicate human learning, progressively refining system accuracy. Thanks to advancements in technology, products grounded in ML, like Netflix's recommendation system and self-driving cars, have emerged in recent years. ML plays a pivotal role in the expanding realm of data science. In data mining endeavours, algorithms are employed to learn patterns and statistics, enabling classification, prediction, and valuable insights. ML encompasses diverse algorithm types, including reinforcement learning, unsupervised learning, and supervised learning. Unlike unsupervised learning which identifies patterns from unlabeled data, supervised learning trains models using labeled data. For models to make decisions based on external input, reinforcement learning comes into play. The journey to building an ML model begins with collecting and preparing data—this involves removing outliers and dividing data into training and testing sets. The choice of an appropriate ML algorithm and tuning its hyperparameters is pivotal for enhanced performance. Model performance is assessed through testing with a dedicated dataset before real-world deployment. ML finds applications across numerous fields, from voice and image recognition to language processing, fraud detection, recommendation systems, and autonomous vehicles. It has the potential to revolutionize industries and significantly improve quality of life.

3.1.1. Artificial neural network (ANN)

An ANN is a computational and mathematical model inspired by how biological nervous systems process information, similar to how our brains work. In an ANN, artificial neurons are created to replicate the behaviors of real neurons and are interconnected. These neurons possess the ability to overcome certain challenges. While addressing AI problems, an ANN doesn't necessarily need to replicate an actual biological system. There are two methods to train an ANN: supervised and unsupervised. In supervised training, the network is given desired outcomes, either by manually evaluating its performance or by matching expected outputs with inputs. Unsupervised training implies that inputs must be interpreted independently by the network. The majority of the networks are using supervision training. Inputs are characterized by an independent training process at the beginning [26]. Neural networks have many applications in the context of large datasets [27]. Backpropagation is a technique used to train ANNs, which involves reducing the weight of neuron connections across networks to compensate for anticipated output and actual outputs. To do this, an error will be returned through a network and each neuron's weight is changed to reduce the error. In general, the ANN is an effective tool for simulating complex systems and understanding them.

3.1.2. Gaussian process regression (GPR)

GPR is a non-parametric statistical method, is used to characterise complex systems that may exhibit nonlinear and nonstationary behaviour. It is based on the notion that any finite collection

of data from a continuous process may be described by a joint multivariate Gaussian distribution. In other words, the fundamental premise of GPR is that the observable data and behaviour of the system are both characterised by a Gaussian process [28]. GPR uses a prior distribution over the possible functions that might potentially explain the data.

In most cases, the prior is a Gaussian distribution over the functions, with a mean function and a covariance function. A prediction is then made using GPR by updating the prior distribution with the observed data to build a posterior distribution. This posterior distribution provides the most current assessment of the various functions that might account for the observed data. The posterior distribution may be used to make predictions for additional input points by accounting for the uncertainty in the function's estimations at those places. The covariance function choice is important in GPR since it influences the function's smoothness and correlations. GPR has a number of advantages over conventional regression approaches, including the ability to quantify estimate uncertainty and the ability to capture nonlinearity and nonstationary data. However, it can be computationally expensive for large datasets since it requires the inversion of a covariance matrix. Numerous approximation techniques, such as sparse GPR and variation GPR, have been developed to address this issue [29].

3.1.3. Support vector regression (SVR)

SVR is a ML technique employed in RA. It's a type of predictive modeling geared towards predicting continuous numerical values rather than discrete categories. SVR stems from SVMs, which are commonly used for solving classification problems. SVMs are widely recognized ML tool, used for both classification and regression tasks. Their primary purpose is to locate a hyperplane that effectively divides input data into distinct groups. The core aim of SVM is to identify the hyperplane with the most significant gap, or margin, between it and the closest data points from different classes. SVM operates by transforming input data into a higher-dimensional feature space using a kernel function. This technique enables SVM to establish non-linear decision boundaries in the original input space, offering flexibility in modeling complex relationships. SVM is a binary classifier, which means that it can only split data into two classes. However, SVM may be expanded to multi-class classification using a one-vs.-all or pairwise technique [30,31].

4. Work methodology

By conducting an extensive review of the existing literature, the experimental database for this study was based on the corroded and FRP-strengthened RC columns. The compilation included 102 specimens, meticulously selected to develop the ML models.

The concentric-loaded reinforced specimens in the database were first cast normally, subjected to various forms of artificial corrosion, and then entirely covered with FRP sheets with the exterior facing in the direction of the hoops. Fig. 1 shows the different layers of the FRP-strengthened RC columns.

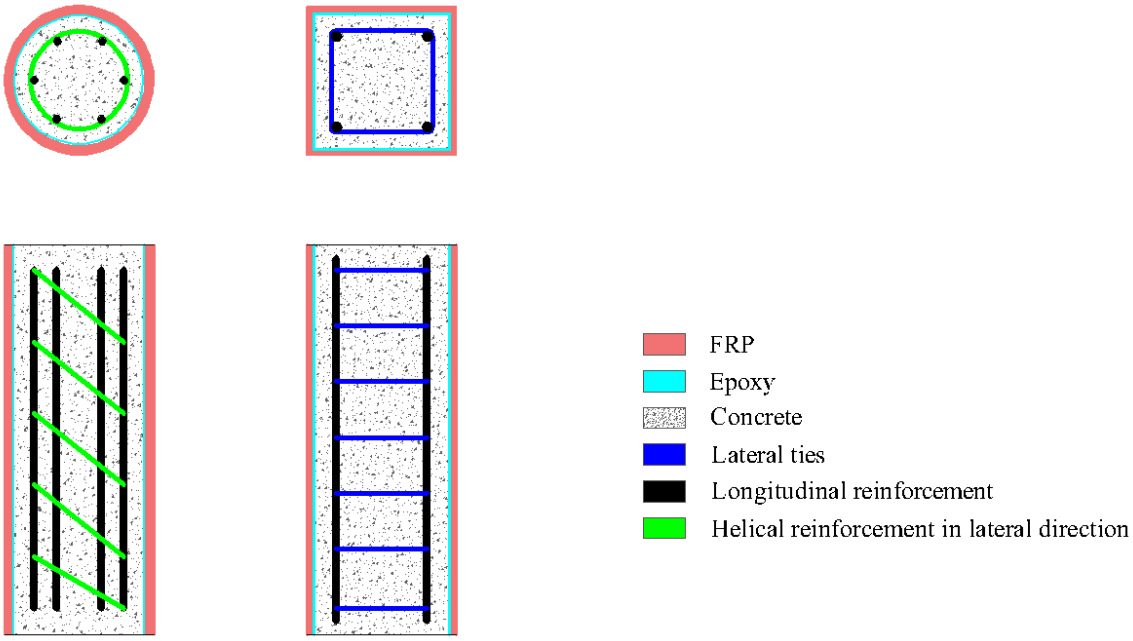

Fig. 1. RC columns wrapped with FRP.

The data consists of 15 input parameters which describes geometrical properties of columns, reinforcement details, FRP properties and corrosion percentage whereas output variable comprises of axial strength of the corroded and FRP-wrapped RC column as described in Table 1. The database varies in various properties like the cross-sectional shape and size of the specimen, type, thickness, and properties of FRP used, and grade of concrete used to make the specimen. The details of the collected dataset along with individual reference is summarised in Table 2. The statistical metrics (minimum, maximum, mean, and SD) of the collected dataset is shown in Table 3. To accomplish the goal of this study, the methodology chart shown in Fig. 2 is applied.

Table 1
Details of parameters utilized.

Parameter	Symbol	Unit
Height of the column	H	mm
The gross cross-sectional area of the column	A_g	mm^2
Compressive strength of concrete	f'_c	N/mm^2
percentage of longitudinal steel in a column	ρ_L	%
Yield strength of longitudinal steel	f_y	N/mm^2
Type of tie	T_{type}	—
Diameter of lateral ties	d_s	mm
c/c spacing of lateral ties	S_v	mm
Yield strength of transverse steel	f_v	N/mm^2
Modulus of Elasticity of FRP	E_f	GPa
Tensile strength of FRP	f_t	MPa
Number of FRP layers	n	—
Thickness of FRP	t_f	mm
Corrosion percentage	η	%
Type of Fabric	F_t	—
Axial strength of the column	P_u	kN

4.1. Standardization

The process of standardization plays a crucial role in the ML algorithms. The standardisation ensure that the dataset must be dimensionless which enhance the interpretability of the ML algorithms. In this work, the normalization was executed within the range of -1 to +1. It helps ML algorithms to achieve computational stability and accuracy. The following expression is used for standardisation of the data.

$$C_{normalized} = \left[2 \times \frac{g - g_{min}}{g_{max} - g_{min}}\right] - 1 \quad (1)$$

where, $C_{normalised}$ stands for normalised value, g is the value to be normalized, g_{max} is the maximum value in the dataset, and g_{min} is the minimum value of the selected dataset.

4.2. Splitting of data

The division of a processed dataset into training and testing sets, with percentages of 80% and 20% respectively, holds significant importance in the field of ML algorithms and data analysis. This allocation serves crucial purposes in developing robust and generalized models. The larger training set allows models to learn intricate patterns, enhancing their ability to comprehend complex relationships within the data. This separation also helps identify overfitting, where models might memorize noise rather than grasp actual patterns.

Table 2
Details of collected database.

Ref.	Specimen	Ag/H	f'_c	ρ_L	f_y/f_v	S_v/d_s	E_f/f_t	$n*t_f$	$\eta(\%)$	$T_{type}*F_t$	P_u
[14]	6	26.18	33.60	2.16	1	13.75	57.5	0.167-0.334	8.89-28.95	1	441-742
[15]	7	35.41-39.77	21-34	1.17-1.75	0.99	3.91-6.76	60.158	0.17	20-36	1	645-1926
[16]	2	71.91	23.50	1.45	0.99	8.80	67.647	0.334	8.50-9.30	1	3547-3659
[17]	5	48.40-49.09	30.50	1.64-1.66	2	5	16	3	25-50	4	1271-2298
[18]	6	58.91	38.47	2.56	0.75	16.67	70.588	0.167	10-35	2	477-1039
[19]	13	125	30	1.13	1.67	21.54	50-67.14	0.26-0.68	5.53-7.92	2-4	1510.60-2333.40
[20]	18	58.91	29.80	1.78	0.99	16.67	82.12-130.70	0.13-0.34	15.00	2-4	473.59-1175.15
[22]	6	58.91	40.50	1.34	0.99	8.33	50	1.7-3.4	5.35-15.55	2	847-1617
[32]	15	19.64	31.50	2.56	0.99	11.67	55.86-60.69	0.26-0.34	15.44-26.60	2-4	209.50-1287
[33]	4	39.71	21	1.17	1	6.76	59.894	0.16	20.00	1	645-774
[34]	12	58.91	39.10	0.89	1.25	22.5	65.671	0.13-0.39	5-10	2	1191.94-2281.21
[35]	8	59.50	50	1.56	0.99	5.26	104.167	1.3	10.00	2	962-1110

Table 3
Statistical parameters of the database.

Parameter	A_g/H	f'_c	ρ_L	f_y/f_v	S_v/d_s	E_f/f_t	$n*t_f$	η (%)	$T_{type}*F_t$	P_u
Min.	19.635	21	0.89	0.749	3.906	16	0.13	5	1	209.5
Max.	125	50	2.56	2	22.5	130.702	3.4	50	4	3659
Mean	57.245	33.461	1.670	1.146	13.804	68.476	0.625	15.963	2.441	1131.767
SD	30.100	7.006	0.565	0.310	6.168	23.695	0.875	9.995	1.122	679.902

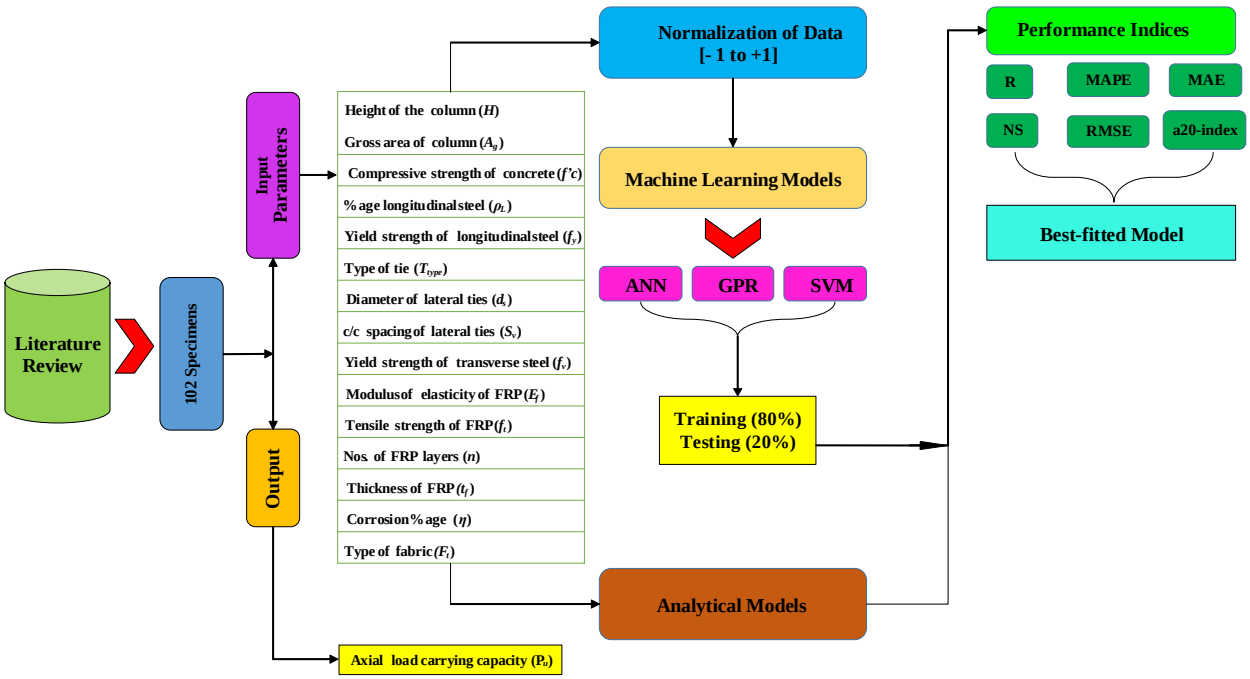

Fig. 2. Methodology chart.

4.3. Performance metrics

To measure the effectiveness and accuracy of ML models and existing design guidelines, performance indicators are employed. Common metrics used for evaluating performance include the correlation coefficient (R), a20-index, MAE, RMSE, MAPE, and Nash-Sutcliffe efficiency index (NS). To evaluate errors, metrics like MAPE, MAE, and RMSE are employed. Achieving lower values for these errors results in higher correlation coefficients (R), ultimately enhancing the accuracy and overall performance of the ML models [36–40]. An indication of a strong positive correlation between the models is suggested by values close to one for R, NS, and the a20-index. Equations 2 to 7 present the mathematical formulations of the performance indices.

$$R = \frac{\sum_{i=1}^{N}(j_i-\bar{j})(k_i-\bar{k})}{\sqrt{\sum_{i=1}^{N}(j_i-\bar{j})^2 \sum_{i=1}^{N}(k_i-\bar{k})^2}} \tag{2}$$

$$MAE = \frac{1}{N}\sum_{i=1}^{N}|j_i - k_i| \tag{3}$$

$$RMSE = \sqrt{\frac{1}{N}\sum_{i=1}^{N}(j_i - k_i)^2} \tag{4}$$

$$MAPE = \frac{1}{N}\sum_{i=1}^{N}\left|\frac{j_i-k_i}{j_i}\right| \times 100 \tag{5}$$

$$NS = 1 - \frac{\sum_{i=1}^{N}(j_i-k_i)^2}{\sum_{i=1}^{N}(j_i-\bar{k})^2} \tag{6}$$

$$a20 - index = \frac{m20}{N} \tag{7}$$

where, j and k are the experimental and predicted output sets, respectively, while $\bar{j}$ and $\bar{k}$ are the means of the experimental and predicted output sets, respectively. N represents the number of values in the dataset, and *m20* is defined as the number of values obtained from measured values divided by predicted values that falls in the range of 0.8 to 1.2.

4.4. Standard guidelines

4.4.1. ACI 440.2R-08

As stated in the ACI 440.2R-08 code [23], which offers guidance on designing and implementing external FRP systems to enhance concrete structures, the axial compressive strength of a sturdy, regular-weight concrete component confined with an FRP jacket can be determined by considering the confined concrete strength. To calculate the axial compressive strength, the reduction factors for strength specified by ACI 318-05 for spiral and tied members need to be taken into account [24].

Therefore, for non-prestressed members with existing steel spiral reinforcement:

$$\phi P_n = 0.85\phi\left[0.85f'_{cc}\left(A_g - A_{st}\right) + f_y A_{st}\right] \tag{8}$$

For non-prestressed members with existing steel-tie reinforcement:

$$\phi P_n = 0.8\phi\left[0.85f'_{cc}\left(A_g - A_{st}\right) + f_y A_{st}\right] \tag{9}$$

where, ϕ = strength reduction factor; P_n = nominal axial compressive strength of a concrete section f'_{cc}= Compressive strength of confined concrete; A_g= Gross area of concrete section; A_{st}= total area of longitudinal reinforcement and f_y= specified yield strength of non-prestressed steel reinforcement.

4.4.2. ACI 318R-05

As per the guidelines outlined in the structural concrete building code (ACI 318-05) and commentary (ACI 318R-05) [24], the design axial strength ϕP_n of compression members (shall not be taken greater than $\phi P_{n,max}$), computed by:

For structural elements without prestressing, but with spiral reinforcement:

$$\phi P_{n,max} = 0.85\phi\left[0.85f'_{c}\left(A_g - A_{st}\right) + f_y A_{st}\right] \tag{10}$$

For structural components without prestressing but containing tie reinforcement:

$$\phi P_{n,max} = 0.80\phi\left[0.85f'_{c}\left(A_g - A_{st}\right) + f_y A_{st}\right] \tag{11}$$

where, $P_{n,max}$ stands for the highest acceptable value of P_n and f'_c represents the compressive strength of concrete.

4.4.3. IS 456:2000

According to IS 456:2000 code [25], plain and RC – code of practice, when the minimum eccentricity remains within 0.05 times the lateral dimension, you can design the members using the following equation:

$$P_u = 0.4f_{ck}A_C + 0.67f_yA_{st} \quad (12)$$

The strength of compression elements featuring helical reinforcement that meets the criteria in section 39.4.1 should be considered as 1.05 times the strength of equivalent elements with lateral ties.

where, P_u stands for the axial load on the element; f_{ck} represents the characteristic compressive strength of the concrete and A_C denotes the area of the concrete.

5. Results and discussion

This section presents the outcomes obtained from both ML models and design guidelines, predicated upon performance matrices encompassing R, a20-index, NS, MAPE, RMSE, and MAE values. These results collectively facilitate the identification of the most optimal ML model and design guideline. Visualization of model outputs has been achieved through the deployment of scatter plots, error plot, and Taylor plot.

5.1. Performance of design guidelines

Table 4 shows the values of performance indicators of the existing design guidelines. The model is considered to be the best which has the lowest values of MAE, RMSE, MAE, and the highest value of R, a20-index, and NS. Model 3 exhibited the best performance having the lowest prediction errors with MAPE, RMSE, and MAE values of 32.19%, 544.72 kN, and 409.94 kN, and highest values of R (0.8478), a20-index (0.2647), and NS (0.5083), respectively. The next optimal recognized model is Model 2 with a value of R (0.8190), a20-index (0.0980), NS (0.3023), MAPE (46.20%), RMSE (746.02 kN), and MAE (584.10 kN). Table 4 also depicts that Model 1 yielded the highest prediction errors of values MAPE (61.30%), RMSE (906.05 kN), MAE (742.07 kN), and least values of R (0.8125), a20-index (0) and NS (0.1859).

Fig. 3 shows a scatter diagram that depicts the comparison between the $P_{u,ped}$ (predicted value), and $P_{u,exp}$ (observed value) for the existing design guidelines. The best-fit line illustrates how well the predicted and actual axial load capacities of corroded and FRP-strengthened RC columns match up. When all the data points align in a single line, it indicates a perfect and complete correlation.

Table 4
Results of design guidelines.

Design guideline	Model	Values					
		R	a20-index	NS	MAPE (%)	RMSE (kN)	MAE (kN)
IS 456:2000	Model 1	0.8125	0	0.1859	61.30	906.05	742.07
ACI 318-05	Model 2	0.8190	0.0980	0.3023	46.20	746.02	584.10
ACI 440.2R-08	Model 3	0.8478	0.2647	0.5083	32.19	544.72	409.94

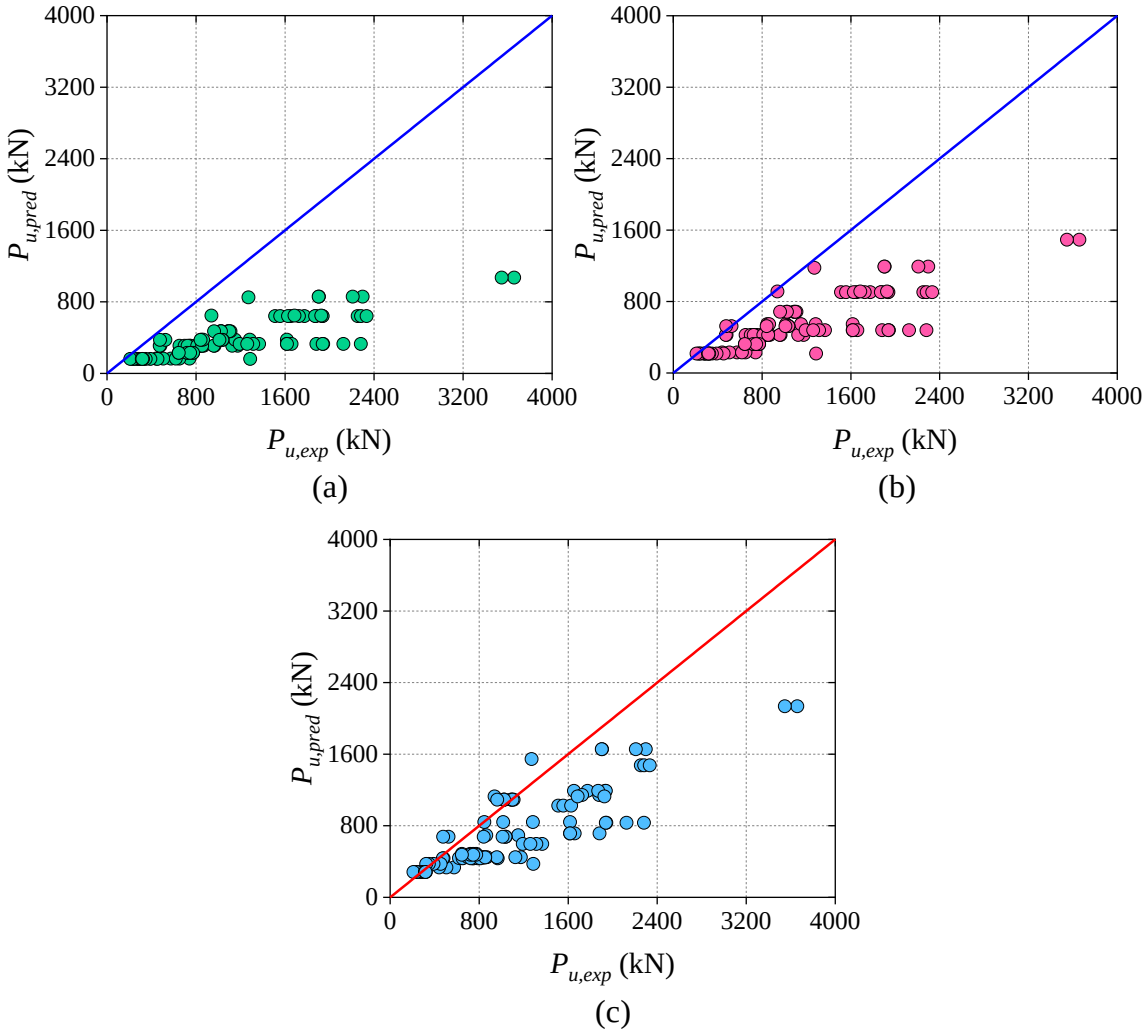

Fig. 3. Results of design guidelines (a) IS 456:2000, (b) ACI 318-05, and (c) ACI 440.2R-08.

In Fig. 3a all the data points are positioned below the diagonal line. This suggests that the model predicts a lower axial capacity for the corroded and FRP-strengthened RC column. Similarly, in Fig. 3b, while some data points come closer to the best-fit line, most of them remain situated beneath the diagonal line. This highlights that the model consistently underestimates the axial capacity of the corroded and FRP-strengthened RC column. However, when compared to the other models shown in Fig. 3c, a notable quantity of data points not only adhere closely to the best-fit line but also exhibit a predominant alignment along the diagonal line. This distinctive pattern significantly enhances the model's remarkable precision in forecasting the axial capacity of corroded and FRP-strengthened RC columns.

5.2. Performance of ML models

In this section, the performance of three ML models – namely, ANN, GPR, and SVM – has been discussed. These models were employed to predict the axial capacity of corroded and FRP-strengthened RC columns. The ANN model's training phase involved exploring a range of hidden

layer neuron counts, from three to twenty-three. By assessing the R and MSE values, it was determined that the optimal number of neurons in a single hidden layer was eighteen. The R-values for the training, testing, and overall dataset were 0.9836, 0.9719, and 0.9808, respectively, as shown in Table 5. Additionally, the performance metrics for the ANN training set included an a20-index of 0.8902, an NS of 0.9674, a MAPE of 8.90%, an RMSE of 123.26 kN, and a MAE of 75.74 kN. However, the error values of the testing set are 12.50%, 165.84 kN, and 111.42 kN for MAPE, RMSE, and MAE, respectively that is higher as compared to the training set. The a20-index and NS values of the testing data set are 21.37% and 3.44% lesser than the training set, respectively. Furthermore, the values of MAPE, RMSE, and MAE of all datasets are 9.60%, 132.69 kN, and 82.74 kN, respectively.

In the GPR model, the training set has the highest R-value of 0.9826 when compared with the testing set with a value of 0.9720. The a20-index, NS, MAPE, RMSE, and MAE of the GPR training model are 0.8780, 0.9646, 9.59%, 128.44 kN, and 83.69 kN, respectively. Moreover, the error values of the testing set are 12.91%, 190.47 kN, and 130.73 kN for performance indices of MAPE, RMSE, and MAE, respectively. The a20-index and NS of the testing data set are 14.58% and 5.34% lesser than the training set, respectively. Furthermore, the values of MAPE, RMSE, and MAE of the whole dataset are 10.24%, 142.74 kN, and 92.92 kN, respectively.

In the case of SVM model, the training set has the highest R-value of 0.9799 when compared with testing and whole datasets with values of 0.9767 and 0.9791, respectively. The a20-index, NS, MAPE, RMSE, and MAE of the SVM training set are 0.9024, 0.9601, 10.14%, 136.35 kN, and 86.67 kN, respectively. Moreover, the error values in the testing set are 11.99%, 144.81 kN, and 106.61 kN for the performance indices of MAPE, RMSE, and MAE, respectively.

The a20-index and NS values of the testing data set are 22.43% and 1.11% lower than the training set. Furthermore, the values of MAPE, RMSE, and MAE of all datasets are 10.50%, 138.05 kN, and, 90.58 kN, respectively.

Table 5
Results of ML models.

Model		Values						SD
		R	a20-index	NS	MAPE (%)	RMSE (kN)	MAE (kN)	
ANN	Training	0.9836	0.8902	0.9674	8.90	123.26	75.74	664.60
	Testing	0.9719	0.700	0.9341	12.50	165.84	111.42	
	All	0.9808	0.8529	0.9615	9.60	132.69	82.74	
GPR	Training	0.9826	0.8780	0.9646	9.59	128.44	83.69	636.26
	Testing	0.9720	0.7500	0.9131	12.91	190.47	130.73	
	All	0.9786	0.8529	0.9555	10.24	142.74	92.92	
SVM	Training	0.9799	0.9024	0.9601	10.14	136.35	86.67	668.55
	Testing	0.9767	0.700	0.9494	11.99	144.81	106.61	
	All	0.9791	0.8627	0.9584	10.50	138.05	90.58	

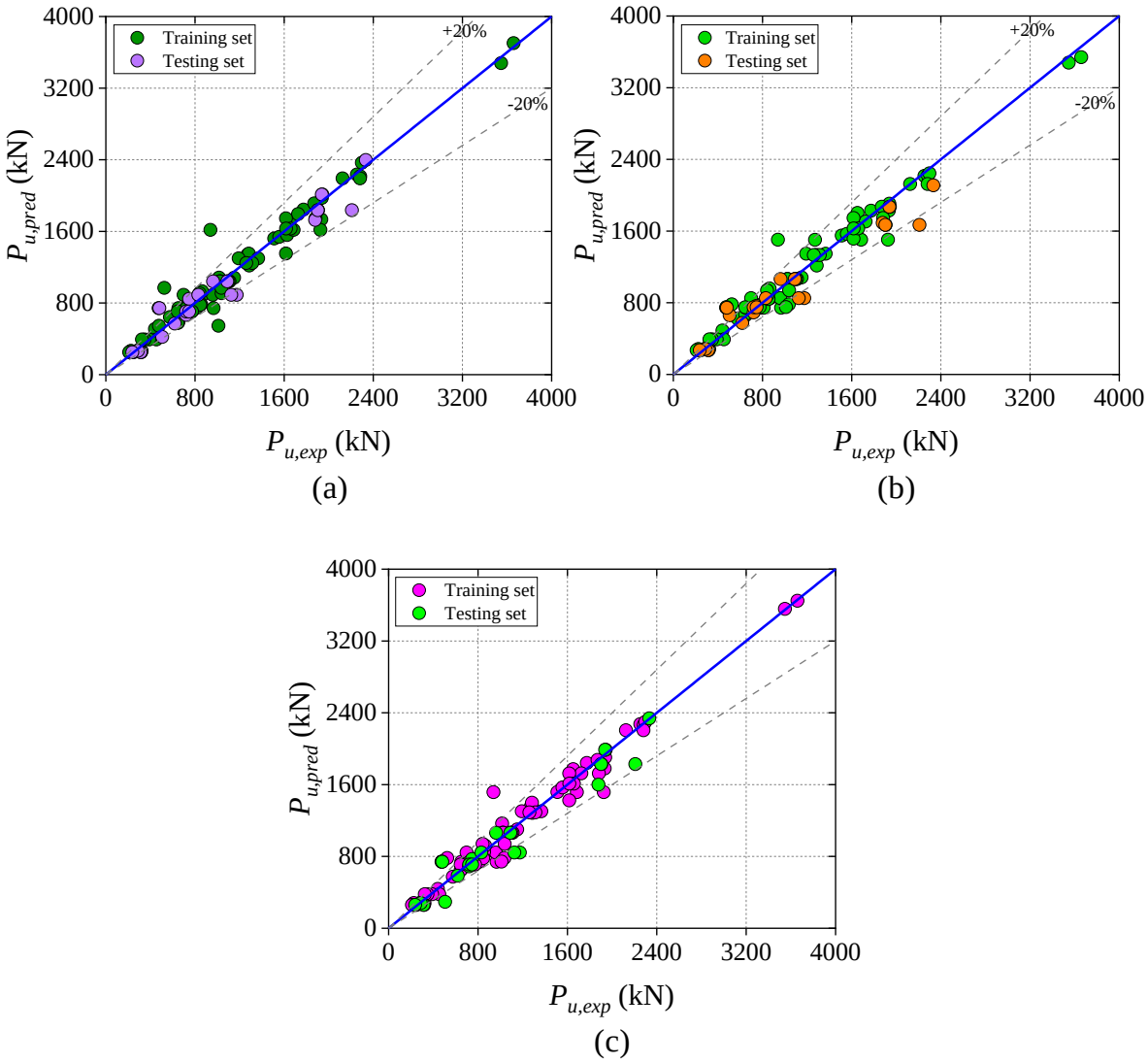

Fig. 4. Results of ML models (a) SVM, (b) GPR, and (c) ANN.

Fig. 4 shows a scatter plot between the $P_{u,ped}$ which is the evaluated value from ML models and the observed value $P_{u,exp}$ from experiments. The blue-coloured best-fit line depicts the relationship between the predicted and actual axial load capacities of corroded and FRP-strengthened RC columns.

Fig. 4 depicts the scatter plot of SVM (Fig. 4a), GPR (Fig. 4b), and ANN (Fig. 4c) models and shows the values fall between -20% and +20% range. Both the predicted and experimental values effectively comply with each other, which depicts that the best line for the ANN model is almost approaches to its identity.

5.3. Comparison between design guidelines and developed ML models

In this section, a thorough comparison has been provided, contrasting the existing design guidelines with the developed ML models. This comparison is aimed at evaluating how well these models estimate the axial capacity of corroded and FRP-strengthened RC columns. This

evaluation is underpinned by an array of performance metrics. To vividly illustrate the findings, error and Taylor plot have been employed.

Table 6
Comparison between design guidelines with proposed ML models.

Model	R	a20-index	NS	MAPE (%)	RMSE (kN)	MAE (kN)
Model-1	0.8125	0	0.1859	61.30	906.05	742.07
Model-2	0.8190	0.0980	0.3023	46.20	746.02	584.10
Model-3	0.8478	0.2647	0.5083	32.19	544.72	409.94
ANN	0.9808	0.8529	0.9615	9.60	132.69	82.74
GPR	0.9786	0.8529	0.9555	10.24	142.74	92.92
SVM	0.9791	0.8627	0.9584	10.50	138.05	90.58

Table 6 shows that the ANN model boasts the highest R-value at 0.9808. This value is superior by 0.22%, 0.17%, 20.71%, 19.76, and 15.69% compared to GPR, SVM, Model-1, Model-2, and Model-3, respectively. Moreover, the MAPE value of the ANN model is 6.25%, 8.57%, 84.34%, 79.22%, and 70.18% lower than GPR, SVM, Model-1, Model-2, and Model-3, respectively. When it comes to RMSE and MAE values, the ANN model showcases the lowest figures at 132.69 kN and 82.74 kN, respectively. This performance is superior to both design guidelines and other developed ML models. The ANN model's NS value is noted as 0.9615, marking it as the highest among all the models. The SVM model stands as the second-best option, with its R, a20-index, and NS values exceeding Model-3 by 15.48%, 225.92%, and 88.55%, respectively. The SVM model also exhibits notably lower MAPE, RMSE, and MAE values, with reductions of 67.38%, 74.66%, and 77.90% compared to Model-3, respectively. Similarly, the GPR model displays lower MAPE, RMSE, and MAE values, showcasing reductions of 68.19%, 73.80%, and 73.33% in comparison to Model-3. In terms of R, a20-index, and NS, the GPR model outperforms Model-3 by 15.43%, 222.21%, and 87.98%, respectively. Comparatively, Model-1 and Model-2 present significantly higher RMSE and MAE values, exceeding the ANN model by 582.83% and 796.87%, and by 462.28% and 605.95%, respectively.

Visual representation is important because it enhances understanding, saves time, enables comparison, and provides clarity. Fig. 5 represents the violin plot and reveals the comparison of the both design guidelines and ML models based on the range of error. This figure shows that the ANN model has the narrowest range of errors when compared to the other models. This leads to the conclusion that the ANN model is the most precise and accurate in predicting the axial load capacity of corroded and FRP-strengthened RC columns. Additionally, the GPR model's range of error is quite similar to that of ANN. On the other hand, the plot also indicates that Model 1 has the broadest range of errors, spanning from around -450 to 2800.

Fig. 6 displays Taylor's diagram, a mathematical representation that visually depicts the connection between predicted and experimental values using SD, R, and RMSE. In the diagram, the dotted green line corresponds to the SD of the entire dataset, while the blue line indicates the RMSE value. In Fig. 6, various models are represented with the help of dots where each colour

represents different models. The position of the dot should correspond with the reference point, which is close to 1 to be an ideal model.

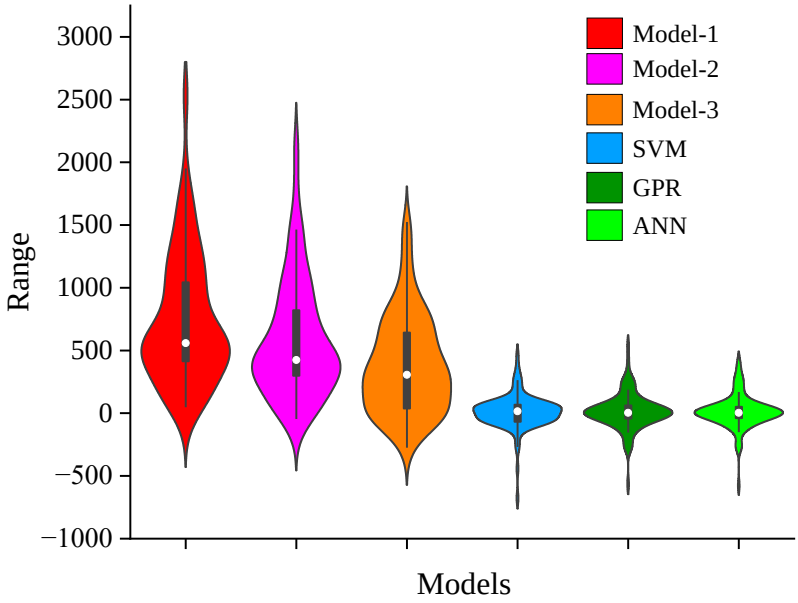

Fig. 5. Error plot of design guidelines as well as ML models.

Taylor plot does not represent results for design guidelines because it was producing wrong results due to lower SD and large RMSE value. Furthermore, the proposed ANN and SVM models are lying and almost conjoining on a green dotted line whereas the GPR model is slightly away from it. Based on this analysis, it's evident that the ANN model outperforms both the SVM and GPR models. As a result, the ANN model stands out as the top-performing choice for accurately predicting the axial capacity of corroded and FRP-strengthened RC columns.

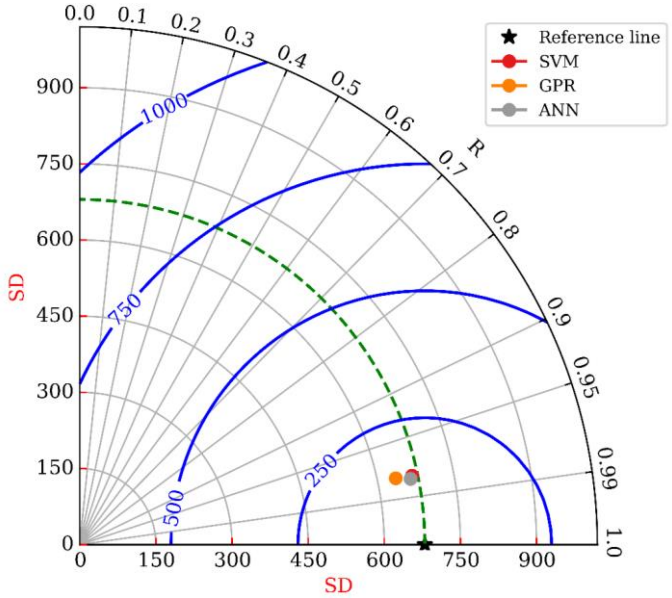

Fig. 6. Taylor plot of design guidelines as well as ML models.

5.4. Sensitivity analysis

This section deliberates on the influence of each input parameter on the axial capacity of corroded and FRP-strengthened RC columns. To understand how the input variables affect the output, we conducted a sensitivity analysis using the method by Milne [41]. The mathematical formula derived from the weight and biases of the created ANN model can be found in the referred works of Liu et al. [42] and Rezazadeh Eidgahee et al. [43]. As illustrated by Fig. 7, P_u of corroded and FRP-strengthened RC columns is mainly affected by the percentage of longitudinal steel in a column (ρ_L) and corrosion percentage (η).

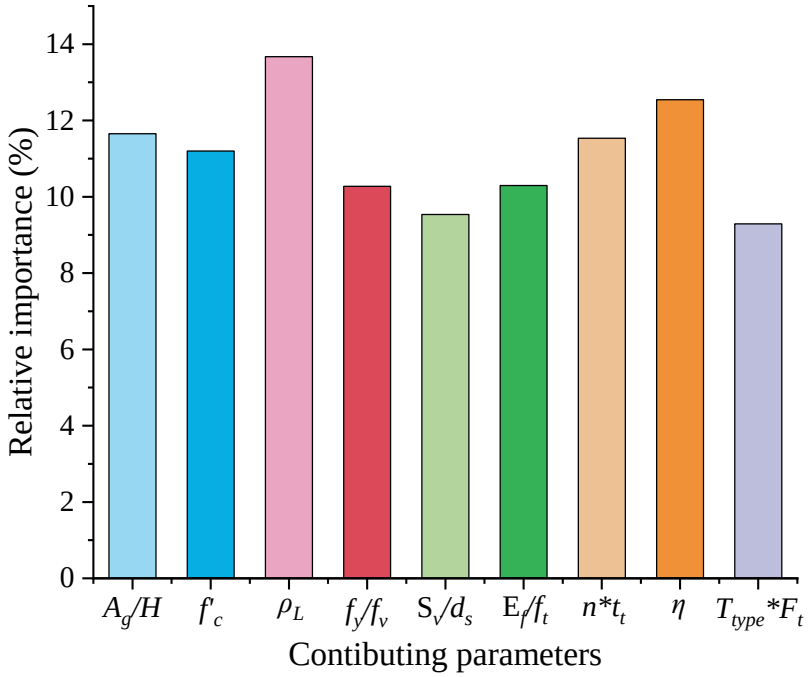

Fig. 7. Sensitivity analysis.

Input parameters that follow next in order of influence are the ratio of gross cross-sectional area of column to the height of the column (A_g/H), the product of the number of FRP layers to the thickness of FRP ($n*t_f$), compressive strength of concrete (f'_c), the ratio of yield strength of longitudinal steel to the yield strength of transverse steel (f_y/f_v), the ratio of modulus of elasticity of FRP to the tensile strength of FRP (E_f/f_t), the ratio of c/c spacing of lateral ties to the diameter of lateral ties (S_v/d_s) and the parameter which least affected the P_u is the product of the type of tie to the type of fabric ($T_{type}*F_t$) respectively.

5.5. ANN-based formulation

The axial load-carrying capacity of the corroded and FRP-strengthened RC columns can be calculated using equation 13 and solved example based on ANN formulation is explained in Appendix A.

$$P_u = f_{(O)} \sum_{i=1}^{N} W_{i(O)} N_i + B_{(O)} \tag{13}$$

where, $W_{i(O)}$ represents the weight in the output layer, $B_{(O)}$ is the output bias, both of which are illustrated in equation 15. The value of N_i can be computed using equation 14.

$$N_i = f_{(H)} \sum_{i=1}^{N} W_{i(H)} X_i + B_{(H)} \tag{14}$$

where, $W_{i(H)}$ denotes the weight in the hidden layer, and $B_{(H)}$ signifies the bias in the hidden layer, as presented in Table 7.

$$P_u = 1.8335Q_1 - 0.2603Q_2 + 0.0297Q_3 - 1.4624Q_4 + 0.3667Q_5 - 1.2146Q_6 + 0.2602Q_7 + 0.2124Q_8 + 1.1315Q_9 - 0.1541Q_{10} - 1.1693Q_{11} - 1.5688Q_{12} + 1.4366Q_{13} - 1.6494Q_{14} - 0.9279Q_{15} + 1.4823Q_{16} - 2.1113Q_{17} + 0.1954Q_{18} - 0.6814 \tag{15}$$

Table 7
Weight and biases of hidden layer.

Neuron					W_H					B_H
1	0.4481	0.1373	-1.0019	1.1312	-1.2100	-0.0214	0.3310	1.5697	1.9372	-1.6681
2	-0.5212	-0.8987	-0.6942	-0.8377	-0.3294	0.5725	-0.1617	0.7355	-0.0970	1.8823
3	1.4541	-0.2412	-0.4604	0.2819	0.9545	0.6015	-1.3492	-0.8410	0.3855	-1.1732
4	-0.7434	-0.8540	1.3925	-0.4101	0.5125	0.6922	0.3195	-0.9134	0.3018	1.4956
5	-0.8158	-1.1186	0.5528	0.8779	-0.7260	-0.6348	0.9238	-0.4450	-0.1169	0.9522
6	-0.0400	0.5918	-0.5688	-0.3440	1.3432	0.8005	-2.3737	1.1804	-1.1377	-2.6912
7	1.4460	2.1774	-1.2237	-1.6314	1.8216	0.4920	-0.8069	-2.0307	1.3728	0.0800
8	1.6939	0.8434	-1.2458	-0.5481	1.3074	-0.2135	-0.0372	-1.9844	-0.0581	-0.4426
9	-0.8836	-0.4157	-1.9395	-1.1669	0.0793	-0.8511	0.0973	-0.0904	-1.0816	0.7698
10	-0.9818	-0.5594	1.1042	-1.6387	0.4800	1.5002	-1.1110	-1.3897	0.0983	-0.5822
11	-1.3325	1.0672	0.5493	0.6465	-0.7690	-0.4809	-0.0958	-0.0356	-1.0581	-0.8505
12	0.2778	-0.8264	-0.0616	1.3727	0.4172	-0.9553	-0.8885	-1.2650	0.7464	0.5491
13	-0.4280	-2.0581	-1.9516	0.1321	-0.0393	1.1680	-1.2471	0.4510	0.4178	0.0212
14	0.4917	-1.2547	-0.4291	0.6923	0.9401	1.2287	-1.5493	0.1417	1.0444	-1.5148
15	-0.8832	-0.7510	1.6535	-1.2821	-0.2143	-0.2704	0.5974	-1.0805	-0.4587	1.4729
16	-0.8153	0.0012	1.9579	-0.0890	1.8541	0.9114	-0.5960	-0.6876	-0.8151	-0.8808
17	-0.9323	-0.3312	0.2471	-0.1277	0.0845	-0.3302	1.3972	1.8271	-1.0326	-1.9972
18	0.6616	-0.5566	-0.7196	0.2994	-0.0947	1.1928	-1.1192	0.2189	-0.2472	1.6751

6. Conclusions

In this study, three ML models were developed to forecast the axial strength of corroded and FRP-strengthened RC columns. These models were formulated using 102 sets of experimental data, incorporating input parameters like A_g, d_s, E_f, f'_c, f_t, F_t, f_v, f_y, H, n, S_v, t_f, T_{type}, ρ_L, η and one output (P_u) gathered from different literature studies. The dataset was randomly split into training and testing sets to construct the ANN, SVM, and GPR models. To assess their dependability, the newly proposed ML models were contrasted with the established design guidelines, considering performance metrics. The results are summarized in the following points for comparison:

- Results show that the ANN model achieved highest precision among all ML models and design guidelines. The R, a20 index, and NS values are 0.9808, 0.8529, and 0.9615, respectively, superior to the design guidelines.
- It has also been concluded that the MAPE, RMSE, and MAE values of the ANN model are 9.60%, 132.69 kN, and 82.74 kN, respectively, which is the lowest among all the models.
- The second-best optimal model is SVM where the value of R, a20-index, and NS values are 15.48%, 225.92%, and 88.55% greater than the Model-3 design guideline.
- The error plot diagram shows that the ANN model has the least range of error whereas Model 1 has the highest range of error, that varies from -450 to 2800 approximately.
- Sensitivity analysis depicts that every input parameter has a different degree of influence where the percentage of steel in the longitudinal direction (ρ_L) has the highest impact on the axial capacity of corroded and FRP-strengthened RC columns followed by the corrosion percentage (η).

The scope of the proposed ML model is limited to values within the input and output ranges. This limitation is an aspect of the current study. Furthermore, in future research, exploring alternative ML algorithms such as the utilization of nature-inspired and metaheuristic algorithms, including but not limited to particle swarm optimization (PSO), ant colony optimization, firefly algorithms, artificial bee colony algorithms, evolutionary algorithms, and artificial swarm intelligence could lead to even more precise and accurate predictions. These algorithms can be employed to optimize the performance of implemented ML models in upcoming studies. Gathering more recent datasets and expanding the range of input and output parameters could enhance the efficiency, reliability, and precision of this model. This, in turn, could contribute to more effective rehabilitation and retrofitting strategies for deteriorated RC structures.

Appendix

$$P_{u,normalized} = 1.8335Q_1 - 0.2603Q_2 + 0.0297Q_3 - 1.4624Q_4 + 0.3667Q_5 - 1.2146Q_6 + 0.2602Q_7 + 0.2124Q_8 + 1.1315Q_9 - 0.1541Q_{10} - 1.1693Q_{11} - 1.5688Q_{12} + 1.4366Q_{13} - 1.6494Q_{14} - 0.9279Q_{15} + 1.4823Q_{16} - 2.1113Q_{17} + 0.1954Q_{18} - 0.6814 \quad \text{(A1)}$$

Considered input parameters are: (normalized values) $\frac{A_g}{H} = -0.8758$, $f_c' = -0.1310$, $\rho_L = 0.5210$, $\frac{f_y}{f_v} = -0.5987$, $\frac{s_v}{d_s} = 0.0588$, $\frac{E_f}{f_t} = -0.2764$, $n * t_f = -0.9774$, $\eta = -0.8271$, $T_{type} * F_t = -1$

The final values of Q_1 to Q_{18} neurons are shown in A1.

Table A1
Values of Q_1 to Q_{18}.

Q_1	Q_2	Q_3	Q_4	Q_5	Q_6	Q_7	Q_8	Q_9	Q_{10}	Q_{11}	Q_{12}	Q_{13}	Q_{14}	Q_{15}	Q_{16}	Q_{17}	Q_{18}
-1	0.9684	-0.8630	0.9967	0.8592	-0.4502	-0.0655	-0.4508	0.9888	0.9987	0.8727	0.7687	-0.3160	-0.9820	0.9999	0.9915	-0.9906	0.8935

$$\begin{bmatrix} Q_1 \\ Q_2 \\ Q_3 \\ Q_4 \\ Q_5 \\ Q_6 \\ Q_7 \\ Q_8 \\ Q_9 \\ Q_{10} \\ Q_{11} \\ Q_{12} \\ Q_{13} \\ Q_{14} \\ Q_{15} \\ Q_{16} \\ Q_{17} \\ Q_{18} \end{bmatrix} = tansig \begin{bmatrix} 0.4481 & 0.1373 & -1.0019 & 1.1312 & -1.2100 & -0.0214 & 0.3310 & 1.5697 & 1.9372 \\ -0.5212 & -0.8987 & -0.6942 & -0.8377 & -0.3294 & 0.5725 & -0.1617 & 0.7355 & -0.0970 \\ 1.4541 & -0.2412 & -0.4604 & 0.2819 & 0.9545 & 0.6015 & -1.3492 & -0.8410 & 0.3855 \\ -0.7434 & -0.8540 & 1.3925 & -0.4101 & 0.5125 & 0.6922 & 0.3195 & -0.9134 & 0.3018 \\ -0.8158 & -1.1186 & 0.5528 & 0.8779 & -0.7260 & -0.6348 & 0.9238 & -0.4450 & -0.1169 \\ -0.0400 & 0.5918 & -0.5688 & -0.3440 & 1.3432 & 0.8005 & -2.3737 & 1.1804 & -1.1377 \\ 1.4460 & 2.1774 & -1.2237 & -1.6314 & 1.8216 & 0.4920 & -0.8069 & -2.0307 & 1.3728 \\ 1.6939 & 0.8434 & -1.2458 & -0.5481 & 1.3074 & -0.2135 & -0.0372 & -1.9844 & -0.0581 \\ -0.8836 & -0.4157 & -1.9395 & -1.1669 & 0.0793 & -0.8511 & 0.0973 & -0.0904 & -1.0816 \\ -0.9818 & -0.5594 & 1.1042 & -1.6387 & 0.4800 & 1.5002 & -1.1110 & -1.3897 & 0.0983 \\ -1.3325 & 1.0672 & 0.5493 & 0.6465 & -0.7690 & -0.4809 & -0.0958 & -0.0356 & -1.0581 \\ 0.2778 & -0.8264 & -0.0616 & 1.3727 & 0.4172 & -0.9553 & -0.8885 & -1.2650 & 0.7464 \\ -0.4280 & -2.0581 & -1.9516 & 0.1321 & -0.0393 & 1.1680 & -1.2471 & 0.4510 & 0.4178 \\ 0.4917 & -1.2547 & -0.4291 & 0.6923 & 0.9401 & 1.2287 & -1.5493 & 0.1417 & 1.0444 \\ -0.8832 & -0.7510 & 1.6535 & -1.2821 & -0.2143 & -0.2704 & 0.5974 & -1.0805 & -0.4587 \\ -0.8153 & 0.0012 & 1.9579 & -0.0890 & 1.8541 & 0.9114 & -0.5960 & -0.6876 & -0.8151 \\ -0.9323 & -0.3312 & 0.2471 & -0.1277 & 0.0845 & -0.3302 & 1.3972 & 1.8271 & -1.0326 \\ 0.6616 & -0.5566 & -0.7196 & 0.2994 & -0.0947 & 1.1928 & -1.1192 & 0.2189 & -0.2472 \end{bmatrix} \times$$

$$\begin{bmatrix} -0.8758 \\ -0.1310 \\ 0.5210 \\ -0.5987 \\ 0.0588 \\ -0.2764 \\ -0.9774 \\ -0.8271 \\ -1 \end{bmatrix} + \begin{bmatrix} -1.6681 \\ 1.8823 \\ -1.1732 \\ 1.4956 \\ 0.9522 \\ -2.6912 \\ 0.0800 \\ -0.4426 \\ 0.7698 \\ -0.5822 \\ -0.8505 \\ 0.5491 \\ 0.0212 \\ -1.5148 \\ 1.4729 \\ -0.8808 \\ -1.9972 \\ 1.6751 \end{bmatrix} \tag{A2}$$

$$P_{u,normalized} = \left(1.8335 \times (-1)\right) - \left(0.2603 \times (0.9684)\right) + \left(0.0297 \times (-0.8630)\right) - \left(1.4624 \times (0.9967)\right) + \left(0.3667 \times (0.8592)\right) - \left(1.2146 \times (-0.4502)\right) + \left(0.2602 \times (-0.0655)\right) + \left(0.2124 \times (-0.4508)\right) + \left(1.1315 \times (0.9888)\right) - \left(0.1541 \times (0.9987)\right) - \left(1.1693 \times (0.8727)\right) - \left(1.5688 \times (0.7687)\right) + \left(1.4366 \times (-0.3160)\right) - \left(1.6494 \times (-0.9820)\right) - \left(0.9279 \times (0.9999)\right) + \left(1.4823 \times (0.9915)\right) - \left(2.1113 \times (-0.9906)\right) + \left(0.1954 \times (0.8935)\right) - 0.6814 \tag{A3}$$

$$P_{u,normalised} = -0.7888 \tag{A4}$$

$$P_{u,unnormalized} = \left[\frac{-0.7888+1}{2}\right] \times 3449.5 + 209.5 \tag{A5}$$

$$P_{u,unnormalized} = 573.7672\ kN \tag{A6}$$

The predicted axial load carrying capacity of the corroded and FRP-strengthened RC columns is 0.2144% less than the experimental value i.e. ($P_{u,exp}$) 575 kN.

Abbreviations

Acronyms		*Symbols*	
ACI	American concrete institute	A_g	Gross cross-sectional area of column
AI	Artificial intelligence	A_{st}	Total area of longitudinal reinforcement
ANN	Artificial neural network	d_s	Diameter of lateral ties
CFRP	Carbon FRP	E_f	Modulus of elasticity of FRP
FRP	Fiber-reinforced polymer	f'_c	Compressive strength of concrete
GFRP	Glass FRP	f'_{cc}	Compressive strength of confined concrete
GPR	Gaussian process regression	f_t	Tensile strength of FRP
MAE	Mean absolute error	F_t	Type of Fabric
MAPE	Mean absolute percentage error	f_v	Yield strength of transverse steel
ML	Machine learning	f_y	Yield strength of longitudinal steel
MSE	Mean squared error	H	Height of the column
NS	Nash–Sutcliffe efficiency index	n	Number of FRP layers
R	Correlation coefficient	P_u	Axial strength of the column
R^2	Coefficient of determination	S_v	Centre to centre spacing of lateral ties
RA	Regression analysis	t_f	Thickness of FRP
RC	Reinforced concrete	T_{type}	Type of tie
RMSE	Root mean square error	η	Corrosion percentage
SHAP	Shapley additive explanation	ρ_L	Percentage of longitudinal steel in a column
SVR	Support vector regression	φ	Strength reduction factor
XGBoost	eXtreme Gradient Boosting	P_n	Nominal axial compressive strength of a concrete section
SD	Standard deviation		

Funding

This research received no external funding.

Conflicts of interest

The authors declare that there are no conflicts of interest regarding the publication of this paper.

Data availability statement

The data used to support the findings of this study are included within the article.

Authors contribution statement

CG, HCA, AK, PK: Conceptualization; CG, AK, PK: Data curation; CG, AK, PK: Formal analysis; HCA, AK, PK: Investigation; HCA, AK, PK, NRK: Methodology; HCA, AK, PK, MS: Project administration; HCA: Resources; AK, PK, NRK: Software; HCA, AK, PK, MS: Supervision; AK, PK, NRK: Validation; AK, PK: Visualization; CG, AK, PK: Roles/Writing – original draft; HCA, NRK, MS: Writing – review & editing.

References

[1] Kashani MM, Maddocks J, Dizaj EA. Residual Capacity of Corroded Reinforced Concrete Bridge Components: State-of-the-Art Review. J Bridg Eng 2019;24. https://doi.org/10.1061/(ASCE)BE.1943-5592.0001429.

[2] Baji H, Yang W, Li C-Q. Optimal FRP-strengthening strategy for corrosion-affected reinforced concrete columns. Struct Infrastruct Eng 2018;14:1586–97. https://doi.org/10.1080/15732479.2018.1476560.

[3] Fang C, Lundgren K, Plos M, Gylltoft K. Bond behaviour of corroded reinforcing steel bars in concrete. Cem Concr Res 2006;36:1931–8. https://doi.org/10.1016/j.cemconres.2006.05.008.

[4] Jin L, Liu M, Zhang R, Du X. Cracking of cover concrete due to non-uniform corrosion of corner rebar: A 3D meso-scale study. Constr Build Mater 2020;245:118449. https://doi.org/10.1016/j.conbuildmat.2020.118449.

[5] Williamson SJ, Clark LA. Pressure required to cause cover cracking of concrete due to reinforcement corrosion. Mag Concr Res 2000;52:455–67. https://doi.org/10.1680/macr.2000.52.6.455.

[6] Batuwitage C, Fawzia S, Thambiratnam D, Al-Mahaidi R. Durability of CFRP strengthened steel plate double-strap joints in accelerated corrosion environments. Compos Struct 2017;160:1287–98. https://doi.org/10.1016/j.compstruct.2016.10.101.

[7] Kubat T, Al-Mahaidi R, Shayan A. CFRP confinement of circular concrete columns affected by alkali-aggregate reaction. Constr Build Mater 2016;116:98–109. https://doi.org/10.1016/j.conbuildmat.2016.04.123.

[8] Diab SH, Soliman AM, Nokken M. Exterior strengthening for ASR damaged concrete: A comparative study of carbon and basalt FRP. Constr Build Mater 2020;235:117435. https://doi.org/10.1016/j.conbuildmat.2019.117435.

[9] Sezen H, Miller E. Retrofit of Circular Reinforced Concrete Columns Using FRP, Steel and Concrete Jackets. New Horizons Better Pract., Reston, VA: American Society of Civil Engineers; 2007, p. 1–3. https://doi.org/10.1061/40946(248)106.

[10] Naderpour H, Nagai K, Haji M, Mirrashid M. Adaptive neuro-fuzzy inference modelling and sensitivity analysis for capacity estimation of fiber reinforced polymer-strengthened circular reinforced concrete columns. Expert Syst 2019;36. https://doi.org/10.1111/exsy.12410.

[11] Ghanem SY, Elgazzar H. Predicting the behavior of reinforced concrete columns confined by fiber reinforced polymers using data mining techniques. SN Appl Sci 2021;3:170. https://doi.org/10.1007/s42452-020-04136-5.

[12] Raza A, Adnan Raheel Shah S, ul Haq F, Arshad H, Safdar Raza S, Farhan M, et al. Prediction of axial load-carrying capacity of GFRP-reinforced concrete columns through artificial neural networks. Structures 2020;28:1557–71. https://doi.org/10.1016/j.istruc.2020.10.010.

[13] Bakouregui AS, Mohamed HM, Yahia A, Benmokrane B. Explainable extreme gradient boosting tree-based prediction of load-carrying capacity of FRP-RC columns. Eng Struct 2021;245:112836. https://doi.org/10.1016/j.engstruct.2021.112836.

[14] Radhi MS, Hassan MS, Gorgis IN. Carbon fibre-reinforced polymer confinement of corroded circular concrete columns. J Build Eng 2021;43:102611. https://doi.org/10.1016/j.jobe.2021.102611.

[15] Bae S-W, Belarbi A. Effects of Corrosion of Steel Reinforcement on RC Columns Wrapped with FRP Sheets. J Perform Constr Facil 2009;23:20–31. https://doi.org/10.1061/(ASCE)0887-3828(2009)23:1(20).

[16] Lee C, Bonacci JF, Thomas M DA, Maalej M, Khajehpour S, Hearn N, et al. Accelerated corrosion and repair of reinforced concrete columns using carbon fibre reinforced polymer sheets. Can J Civ Eng 2000;27:941–8. https://doi.org/10.1139/l00-030.

[17] Mohammed AA, Manalo AC, Maranan GB, Zhuge Y, Vijay P V., Pettigrew J. Behavior of Damaged Concrete Columns Repaired with Novel FRP Jacket. J Compos Constr 2019;23. https://doi.org/10.1061/(ASCE)CC.1943-5614.0000942.

[18] Zhou YW, Wu LY, Sui LL, Xing F. Experimental Studies on the Mechanical Performances of Corroded Reinforced Concrete Columns Retrofitted with FRP. Appl Mech Mater 2013;405–408:726–30. https://doi.org/10.4028/www.scientific.net/AMM.405-408.726.

[19] Tastani SP, Pantazopoulou SJ. Experimental evaluation of FRP jackets in upgrading RC corroded columns with substandard detailing. Eng Struct 2004;26:817–29. https://doi.org/10.1016/j.engstruct.2004.02.003.

[20] Kashi A, Ramezanianpour AA, Moodi F. Durability evaluation of retrofitted corroded reinforced concrete columns with FRP sheets in marine environmental conditions. Constr Build Mater 2017;151:520–33. https://doi.org/10.1016/j.conbuildmat.2017.06.137.

[21] Debaiky AS, Green MF, Hope BB. Modeling of Corroded FRP-Wrapped Reinforced Concrete Columns in Axial Compression. J Compos Constr 2007;11:556–64. https://doi.org/10.1061/(ASCE)1090-0268(2007)11:6(556).

[22] Pantazopoulou SJ, Bonacci JF, Sheikh S, Thomas MDA, Hearn N. Repair of Corrosion-Damaged Columns with FRP Wraps. J Compos Constr 2001;5:3–11. https://doi.org/10.1061/(ASCE)1090-0268(2001)5:1(3).

[23] Committee ACI. Guide for the Design and Construction of Externally Bonded FRP Systems for Strengthening Concrete Structures (ACI 440.2R-08). Am. Concr. Inst., American Concrete Institute; 2005.

[24] Committee ACI. Building code requirements for structural concrete (ACI 318-05) and commentary (ACI 318R-05), American Concrete Institute; 2005.

[25] Standard I. Plain and reinforced concrete-code of practice. New Delhi Bur Indian Stand 2000.

[26] Naderpour H, Sharei M, Fakharian P, Heravi MA. Shear Strength Prediction of Reinforced Concrete Shear Wall Using ANN, GMDH-NN and GEP. J Soft Comput Civ Eng 2022;6:66–87. https://doi.org/10.22115/SCCE.2022.283486.1308.

[27] Naseri Nasab M, Jahangir H, Hasani H, Majidi M-H, Khorashadizadeh S. Estimating the punching shear capacities of concrete slabs reinforced by steel and FRP rebars with ANN-Based GUI toolbox. Structures 2023;50:1204–21. https://doi.org/10.1016/j.istruc.2023.02.072.

[28] Ghanizadeh AR, Heidarabadizadeh N, Heravi F. Gaussian Process Regression (GPR) for Auto-Estimation of Resilient Modulus of Stabilized Base Materials. J Soft Comput Civ Eng 2021;5:80–94. https://doi.org/10.22115/scce.2021.269187.1273.

[29] Kumar A, Arora HC, Mohammed MA, Kumar K, Nedoma J. An Optimized Neuro-Bee Algorithm Approach to Predict the FRP-Concrete Bond Strength of RC Beams. IEEE Access 2022;10:3790–806. https://doi.org/10.1109/ACCESS.2021.3140046.

[30] Singh R, Arora HC, Bahrami A, Kumar A, Kapoor NR, Kumar K, et al. Enhancing Sustainability of Corroded RC Structures: Estimating Steel-to-Concrete Bond Strength with ANN and SVM Algorithms. Materials (Basel) 2022;15:8295. https://doi.org/10.3390/ma15238295.

[31] Rahul AK, Shivhare N, Kumar S, Dwivedi SB, Dikshit PKS. Modelling of Daily Suspended Sediment Concentration Using FFBPNN and SVM Algorithms. J Soft Comput Civ Eng 2021;5:120–34. https://doi.org/10.22115/scce.2021.283137.1305.

[32] Chenchen LI, Aimin YU, Danying GAO ZP. Experimental study on axial compression of corroded reinforced concrete columns strengthened with FRP strips under erosion environment. Acta Mater Compos Sin 2020;37:2015–28. https://doi.org/http://doi.org/10.13801/j.cnki.fhclxb.20200212.005.

[33] Belarbi A, Bae S-W. An experimental study on the effect of environmental exposures and corrosion on RC columns with FRP composite jackets. Compos Part B Eng 2007;38:674–84.

https://doi.org/10.1016/j.compositesb.2006.09.004.

[34] Xiang Z, Wang J, Niu J, Zhou J, Wang J. Axial compressive responses of concrete canvas and CFRP reinforced corroded concrete short columns. Case Stud Constr Mater 2022;17:e01661. https://doi.org/10.1016/j.cscm.2022.e01661.

[35] Neale KW, Demers M, Labossiere P. FRP protection and rehabilitation of corrosion-damaged reinforced concrete columns. Int J Mater Prod Technol 2005;23:348–71.

[36] Kumar A, Arora HC, Kapoor NR, Kumar K. Prognosis of compressive strength of fly-ash-based geopolymer-modified sustainable concrete with ML algorithms. Struct Concr 2023;24:3990–4014. https://doi.org/10.1002/suco.202200344.

[37] Kumar K, Saini RP. Adaptive neuro-fuzzy interface system based performance monitoring technique for hydropower plants. ISH J Hydraul Eng 2023;29:611–21. https://doi.org/10.1080/09715010.2022.2115320.

[38] Jahangir H, Rezazadeh Eidgahee D. A new and robust hybrid artificial bee colony algorithm – ANN model for FRP-concrete bond strength evaluation. Compos Struct 2021;257:113160. https://doi.org/10.1016/J.COMPSTRUCT.2020.113160.

[39] Suri RS, Jain AK, Kapoor NR, Kumar A, Arora HC, Kumar K, et al. Air Quality Prediction - A Study Using Neural Network Based Approach. J Soft Comput Civ Eng 2023;7:93–113. https://doi.org/10.22115/scce.2022.352017.1488.

[40] Jahangir H, Nikkhah Z, Rezazadeh Eidgahee D, Esfahani MR. Performance Based Review and Fine-Tuning of TRM-Concrete Bond Strength Existing Models. Soft Comput Civ Eng 2023;7:43–55. https://doi.org/10.22115/SCCE.2022.349483.1476.

[41] Milne L. Feature selection using neural networks with contribution measures. Eighth Aust. Jt. Conf. Artif. Intell. AI'95, 1995.

[42] Liu K, Zou C, Zhang X, Yan J. Innovative prediction models for the frost durability of recycled aggregate concrete using soft computing methods. J Build Eng 2021;34:101822. https://doi.org/10.1016/j.jobe.2020.101822.

[43] Rezazadeh Eidgahee D, Jahangir H, Solatifar N, Fakharian P, Rezaeemanesh M. Data-driven estimation models of asphalt mixtures dynamic modulus using ANN, GP and combinatorial GMDH approaches. Neural Comput Appl 2022. https://doi.org/10.1007/s00521-022-07382-3.